Radiology

ORIGINAL RESEARCH • CARDIAC IMAGING

Coronary CT Angiography with Photon-counting CT: First-In-Human Results

*Salim A. Si-Mohamed, MD, PhD** • *Sara Boccalini, MD, PhD** • *Hugo Lacombe, MSc* • *Adja Diaw, MSc* • *Mohammad Varasteh, PhD* • *Pierre-Antoine Rodesch, PhD* • *Riham Dessouky, MD, PhD* • *Marjorie Villien, PhD* • *Valérie Tatard-Leitman, PhD* • *Thomas Bochaton, MD, PhD* • *Philippe Coulon, PhD* • *Yoad Yagil, PhD* • *Elias Lahoud, PhD* • *Klaus Erhard, PhD* • *Benjamin Riche, PhD* • *Eric Bonnefoy, MD, PhD* • *Gilles Rioufol, MD, PhD* • *Gerard Finet, MD, PhD* • *Cyrille Bergerot, MD* • *Loic Boussel, MD, PhD* • *Joel Greffier, PhD* • *Philippe C. Douek, MD, PhD*

From the University Lyon, INSA-Lyon, University Claude Bernard Lyon 1, UJM-Saint Etienne, CNRS, Inserm, CREATIS UMR 5220, U1206, Villeurbanne, France (S.A.S.M., S.B., H.L., A.D., M. Varasteh, P.A.R., V.T.L., L.B., P.C.D.); Departments of Radiology (S.A.S.M., S.B., L.B., P.C.D.) and Cardiology (T.B., E.B., G.R., G.F., C.B.), Louis Pradel Hospital, Hospices Civils de Lyon, Bron, France; Department of Radiology, Faculty of Medicine, Zagazig University, Egypt (R.D.); Philips Healthcare, Suresnes, France (M Villien, P.C.); Philips Healthcare, Haifa, Israel (Y.Y., E.L.); Philips Healthcare, Hamburg, Germany (K.E.); Public Health Center, Department of Biostatistics and Bioinformatics, Hospices Civils de Lyon, Lyon, France (B.R.); Department of Biometrics and Evolutionary Biology Laboratory, Biostatistics-Health Team, CNRS, UMR 5558, Villeurbanne, France (B.R.); and Department of Medical Imaging, CHU Nimes, University Montpellier, Nimes Medical Imaging Group, EA 2992, Montpellier, France (J.G.). Received July 21, 2021; revision requested August 27; revision received September 13; accepted November 4. **Address correspondence to** S.A.S.M. (e-mail: *salim.si-mohamed@chu-lyon.fr*).

Supported by European Union Horizon 2020 grant 643694.

* S.A.S.M. and S.B. contributed equally to this work.

Conflicts of interest are listed at the end of this article.

See also the editorial by Sandfort and Bluemke in this issue.

Radiology 2022; 000:1–11 • https://doi.org/10.1148/radiol.211780 • Content codes: CA CT

Background. Spatial resolution, soft-tissue contrast, and dose-efficient capabilities of photon-counting CT (PCCT) potentially allow a better quality and diagnostic confidence of coronary CT angiography (CCTA) in comparison to conventional CT.

Purpose: To compare the quality of CCTA scans obtained with a clinical prototype PCCT system and an energy-integrating detector (EID) dual-layer CT (DLCT) system.

Materials and Methods: In this prospective board-approved study with informed consent, participants with coronary artery disease underwent retrospective electrocardiographically gated CCTA with both systems after injection of 65–75 mL of 400 mg/mL iodinated contrast agent at 5 mL/sec. A prior phantom task-based quality assessment of the detectability index of coronary lesions was performed. Ultra-high-resolution parameters were used for PCCT (1024 matrix, 0.25-mm section thickness) and EID DLCT (512 matrix, 0.67-mm section thickness). Three cardiac radiologists independently performed a blinded analysis using a five-point quality score (1 = insufficient, 5 = excellent) for overall image quality, diagnostic confidence, and diagnostic quality of calcifications, stents, and noncalcified plaques. A logistic regression model, adjusted for radiologists, was used to evaluate the proportion of improvement in scores with the best method.

Results: Fourteen consecutive participants (12 men; mean age, 61 years ± 17) were enrolled. Scores of overall quality and diagnostic confidence were higher with PCCT images with a median of 5 (interquartile range [IQR], 2) and 5 (IQR, 1) versus 4 (IQR, 1) and 4 (IQR, 3) with EID DLCT images, using a mean tube current of 255 mAs ± 0 versus 349 mAs ± 111 for EID DLCT images ($P < .01$). Proportions of improvement with PCCT images for quality of calcification, stent, and noncalcified plaque were 100%, 92% (95% CI: 71, 98), and 45% (95% CI: 28, 63), respectively. In the phantom study, detectability indexes were 2.3-fold higher for lumen and 2.9-fold higher for noncalcified plaques with PCCT images.

Conclusion: Coronary CT angiography with a photon-counting CT system demonstrated in humans an improved image quality and diagnostic confidence compared with an energy-integrating dual-layer CT.

Online supplemental material is available for this article.

Coronary CT angiography (CCTA) is currently recommended for the assessment of many cardiovascular diseases, including coronary artery disease (CAD) evaluation (1). CCTA is particularly important for its high negative predictive value for CAD in a low- and intermediate-risk acute chest pain population, with a high sensitivity and specificity for CAD in a low- and intermediate-risk chronic coronary syndrome population (2–5). This had been made possible by the recent technical evolution of the CT systems and the existence of large-scale validation cohort studies (6,7). However, conventional CCTA still has a limited spatial resolution and soft-tissue contrast, which impairs its diagnostic performance for small arteries (ie, <2 mm) and high-contrast (eg, stent, calcification) and low-contrast (eg, noncalcified plaque) tasks, and carries the risks of relatively high x-ray dose delivery.

Over the past 5 years, photon-counting CT (PCCT) technology has emerged in the field of CT imaging. Compared with conventional CT, this new modality has better spatial resolution and soft-tissue contrast and reduced noise, blooming, and beam-hardening artifacts (8). This is because of new energy-resolving detectors, called photon-counting

Abbreviations

CAD = coronary artery disease, CCTA = coronary CT angiography, DLCT = dual-layer CT, EID = energy-integrating detector, IQR = interquartile range, NPS = noise power spectrum, PCCT = photon-counting CT, PCD = photon-counting detector, TTF = task transfer function

Summary

Photon-counting CT enables improved image quality and diagnostic confidence for coronary CT angiography examinations at comparable dose, in comparison to an energy-integrating detector dual-layer CT.

Key Results

- In a prospective evaluation of 14 study participants undergoing both coronary photon-counting CT (PCCT) and energy-integrating detector (EID) dual-layer CT angiography, three radiologists found that PCCT had greater diagnostic quality score improvement for 100%, 92%, and 45% of the coronary calcification, stent, and non-calcified plaque cases, respectively.
- In a phantom study, PCCT images in comparison to EID CT images had 2.3- and 2.9-fold increased detectability index for coronary lumen and non-calcified plaque, respectively.

detectors (PCDs), that register separately the energy of each photon, thus allowing a better measurement of the transmitted spectrum (9,10). Moreover, PCDs are made of a smaller pixel size than the energy-integrating detectors (EIDs) used with conventional CT, which limits the pile-up effect, and do not require the coating of each detection pixel by optical reflectors (septa), leading to a theoretical two to three times higher resolution than conventional CT (approximately 250 μm) (10). Altogether, PCCT systems have evolved considerably, with recent developments enabling human imaging (11–15). However, to the best of our knowledge, PCCT has still not been tested with regard to CCTA.

Therefore, in the present study, we aimed to compare the image quality of and diagnostic confidence with CCTA in humans between PCCT and EID dual-layer CT (DLCT).

Materials and Methods

Study Design and Population

This prospective institutional review board–approved study was conducted at a cardiothoracic university hospital (Hôpital Louis Pradel, Hospices Civils de Lyon, France) from January to June 2021 (Hospices Civils de Lyon, approval number: 2019-A02945–52) (Fig 1). Informed consent was obtained. The population consisted of consecutive patients with suspected or known CAD referred for CCTA. Exclusion criteria were as follows: age younger than 18 years, contraindication to iodinated contrast agents, or renal failure with a clearance of 30 mL/min or less.

PCCT and EID DLCT Systems

Both systems used were made by the same manufacturer (Philips Healthcare). The PCCT system is a clinical prototype with a large field of view (500 mm in plane) equipped with a single-layer of energy-sensitive PCDs of 2-mm-thick cadmium zinc telluride with a pixel pitch of 270 × 270 μm^2 at isocenter, bonded to a proprietary ChromAIX2 application-specific integrated circuit (16). Further technical details are provided in Appendix E1 (online).

The EID DLCT system is a clinical dual-layer detector system equipped with two layers of EIDs (IQon CT, Philips Healthcare) that generate conventional images by summing the projection from each layer. A comparison of the technical details of both systems is provided in Table 1.

Clinical Imaging Protocol

CCTA acquisition.—All patients underwent CCTA with both CT systems 3 days apart. CCTA was performed using a standard reference protocol in our institution, which is a retrospective electrocardiographically gated helical acquisition after an injection of a bolus of iomeprol (400 mg/mL; Iomeron, Bracco) at 5 mL/sec via a 20-gauge catheter followed by a saline flush of 20 mL at 4 mL/sec. Bolus volume calculation was adjusted to the weight of the patient (65 mL for patients <80 kg and 75 mL for patients >80 kg). For PCCT, a bolus test was performed using an injection of 20 mL of contrast agent injected at 5 mL/sec followed by a saline flush of 20 mL at 4 mL/sec. For EID DLCT, bolus tracking with a region of interest in the descending aorta using a threshold set at 110 HU was used. Patients received sublingual nitroglycerine (Natispray, Teofarma) and an intravenous beta-blocker (esmolol chlorohydrate [Esmocard, Orpha Devel Handels Vertriebs]) when needed.

Acquisition and reconstruction parameters.—Following manufacturer recommendations and validation by three experienced cardiac radiologists (P.C.D., S.A.S.M., and S.B.,

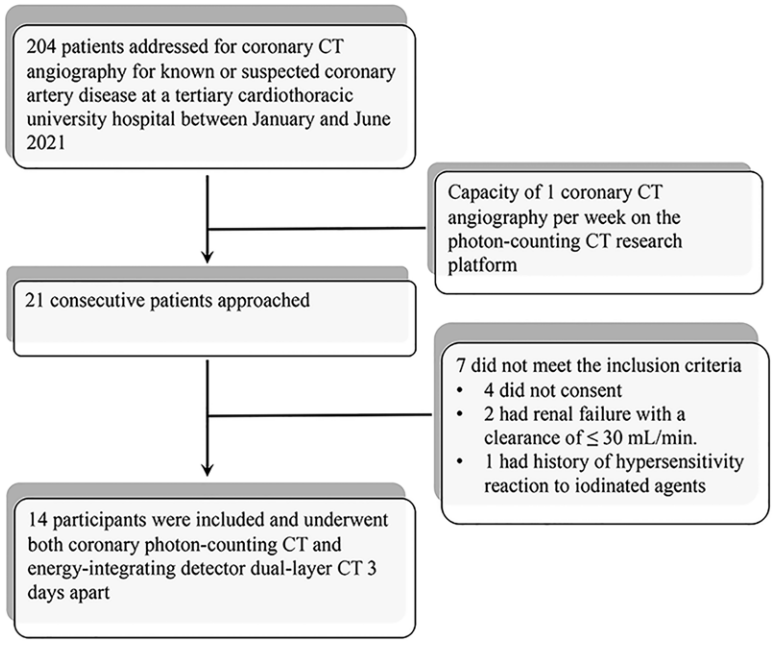

Figure 1: Flowchart of participant enrollment.

with 30, 7, and 7 years of experience, respectively), the acquisition and reconstruction parameters were chosen to convey the best image quality for each system (Table 1). For both systems, the tube voltage was set at 120 kVp with a current fixed at 255 mAs for PCCT, while for EID DLCT automatic exposure control was used with a DoseRight index of 28 corresponding to a target current at 255 mAs for average adult patient size with water equivalent diameter of 29 cm.

Data were reconstructed between the mid-diastolic and systolic phases (40%–78% of the RR interval) of the cardiac cycle using a field of view of 220 mm. Matrix size was increased from 512 to 1024 for PCCT, and section thickness was decreased from 0.67 mm to 0.25 mm for PCCT to convey its intrinsic spatial resolution capabilities, as in a previous study (11). These parameters produced ultra-high-resolution images with a voxel size of 0.25 (z) · 0.21 (x) · 0.21 (y) mm for PCCT, which is close to the size of the detector pixel at isocenter (11). A hybrid iterative reconstruction algorithm (iDose, Philips Healthcare) was used for both systems, with a level set at 3 for EID DLCT and increased at 6 for PCCT because of the higher noise induced by the ultra-high-resolution parameters, which allow, respectively, a decrease of the noise of 25% and 45%, respectively.

Table 1: Acquisition and Reconstruction Parameters

Parameter	PCCT	EID DLCT
Acquisition parameters		
Tube voltage (kVp)	120	120
Tube current (mAs)	No modulation with 255 mAs	Without modulation for phantom imaging; dose right index of 28 (ie, 255 mAs as reference for average adult size)
Rotation time (sec/rotation)	0.33	0.27
Pitch factor	0.32	0.16
Focal spot (mm)	Small (0.6 × 0.7)	Standard (1.1 × 1.2)
Collimation (mm)	64 × 0.275	64 × 0.625
Reconstruction parameters		
iDose[4] levels*	iDose 6	iDose 3
Reconstruction kernel	Detailed 2†	XCB‡
Matrix size (no. of pixels)	1024 × 1024	512 × 512
Field of view (mm)	220	220
Section thickness/ increment (mm)	0.25/0.25	0.67/0.34

Note.—DLCT = dual-layer CT, EID = energy-integrating detector, PCCT = photon-counting CT, XCB = Xres cardiac standard.

* Philips Healthcare.

† Detailed two-filter cut-off is at 14 line pairs per centimeter.

‡ XCB filter cut-off is at 12.7 line pairs per centimeter.

Task-based image quality assessment.—A task-based image quality assessment was performed using the imQuest software to assess the noise magnitude and texture using the noise power spectrum (NPS) and the spatial resolution as function of contrast using the task transfer function (TTF) and to estimate the ability of the radiologist to detect some lesions with the detectability index (d′) (17–23). A 20-cm-diameter ACR CT-464 QA phantom (Gammex) was scanned to measure the NPS (Fig E1A [online]) and the TTF (Fig E1B [online]) using the same acquisition and reconstruction parameters summarized in Table 1.

The TTF on bone and polyethylene inserts and the NPS were computed and combined with a task function to compute the detectability index estimating the detectability of coronary lesions, that is, a higher detectability index corresponds with a greater capability to depict the task (17–22). The coronary lumen was assumed to represent a circular signal with a pre-imaged high contrast of 350 HU and a diameter of 4 mm, and the noncalcified plaque was assumed to be a low contrast of 40 HU and a diameter of 2 mm. TTF results from the polyethylene insert were used for the detection task of the noncalcified plaque, while the results from the bone insert were used for coronary lumen. Interpretation conditions to calculate the detectability index were a zoom factor of 1.5, a 500-mm viewing distance, and a 220 mm field of view. Further details are provided in Appendix E1 (online).

Image quality analysis.—For analysis of objective image quality, all images were reviewed in consensus by three observers on a clinical workstation (IntelliSpace Portal version 12.0, Philips Healthcare). Objective image noise, vessel attenuation, beam hardening, signal-to-noise ratio, and contrast-to-noise ratio of the proximal and distal coronary lumen were analyzed. Details are reported in Appendix E1 (online) along with a specific objective analysis on coronary calcified plaque.

For analysis of subjective image quality, three experienced cardiac radiologists (P.C.D., S.A.S.M., and S.B.) blinded to image type and patient identity reviewed all images independently in a random order. Changes in image and window settings were allowed according to personal preference. The reviewers scored the images independently using a five-point quality score (1 = insufficient, 5 = excellent), according to the criteria defined in previous study (11), for overall quality, diagnostic confidence, overall noise, and diagnostic quality of following structures: coronary wall, proximal and distal lumen, calcification, stent, noncalcified plaque, cardiac muscle, cavities, valves, pericardium, pericoronary and epicardial adipose tissue, and beam-hardening, ring, and metallic artifacts. In addition, sharpness and conspicuity of coronary calcification, stent, noncalcified plaque, and motion artifacts were graded using the same scale. A patient's CT scan was considered of sufficient diagnostic quality if the motion artifact score was greater than 3.

Table 2: Task-based Image Quality Analysis

Parameter	PCCT	EID DLCT
NPS		
Noise magnitude (HU)	23.9 ± 0.4	26.6 ± 0.5
f_{peak} (mm^{-1})	0.05/0.68*	0.20
f_{av} (mm^{-1})	0.56 ± 0.01	0.27 ± 0.01
TTF		
f_{50} of polyethylene insert (mm^{-1})	0.62 ± 0.01	0.32 ± 0.02
f_{10} of polyethylene insert (mm^{-1})	1.08 ± 0.07	0.65 ± 0.04
f_{50} of bone insert (mm^{-1})	0.88 ± 0.01	0.41 ± 0.01
f_{10} of bone insert (mm^{-1})	1.39 ± 0.01	0.71 ± 0.01
Detectability index		
d′ 350 HU-4 mm	41.78 ± 1.44	18.38 ± 0.36
d′ 40 HU-2 mm	2.64 ± 0.06	0.92 ± 0.02

Note.—Except where indicated, data are means ± standard deviations. Noise power spectrum (NPS) assesses the magnitude and texture of the noise, while task transfer function (TTF) assesses the spatial resolution as a function of a given contrast. TTF results from the polyethylene insert were used for the detection task of the noncalcified plaque, whereas the results from the bone insert were used for coronary lumen. TTF and NPS were computed and combined with a task function to compute the detectability index (d') estimating the detectability of coronary lesions. DLCT = dual-layer CT, EID = energy-integrating detector, f_{av} = average NPS spatial frequency, f_{peak} = spatial frequency of the NPS peak, f_{10} = value of TTF at 10%, f_{50} = value of TTF at 50%, PCCT = photon-counting CT.

* Spatial frequencies for the first and second peaks.

Radiation Dose Study

Dose-length product and volume CT dose index were recorded. Further explanation of the technical difference in dose is provided in Appendix E1 (online).

Statistical Analysis

Statistical analysis was performed with the Prism software package (version 9, GraphPad) and R (version 4.0.3, R Foundation for Statistical Computing). The data are expressed as means ± standard deviations for normally distributed variables and as medians and interquartile range (IQR) for nonnormally distributed variables. The continuous variables were compared using a paired two-tailed Student *t* test or Wilcoxon rank-sum test as a function of the normality of the variables. Distributions were tested for normality using the d'Agostino-Pearson test. The Cohen κ coefficient was used to assess the agreement per radiologist between the quality scores of the PCCT and EID DLCT images. A logistic regression model, adjusted for radiologists, was used to evaluate the concordance in subjective quality assessment between the PCCT and EID DLCT images and then to evaluate the proportion of improvement of the quality scores with the best method. The Wald test was used to compare results between radiologists. $P < .05$ was considered indicative of a statistically significant difference. The parameters were considered independent, and no correction for multiple tests was used.

Table 3: Demographic Characteristics of the Study Population

Parameter	Value
No. of participants	14
Mean age (y)	61 ± 17
No. of men*	12 (86)
Mean height (cm)	172 ± 10.0
Mean weight (kg)	74 ± 12
Mean body mass index (kg/m^2)	25 ± 4
Heart rate during EID DLCT (beats/min)	68 ± 8
Heart rate during PCCT (beats/min)	65 ± 12
No. of patients with calcified plaque*	10 (71)
No. of calcified plaques	32
No. of patients with stent*	8 (57)
No. of stents	16
No. of patients with noncalcified plaque*	12 (86)
No. of noncalcified plaques	15

Note.—Unless otherwise indicated, data are means ± standard deviations. DLCT = dual-layer CT, EID = energy-integrating detector, PCCT = photon-counting CT.

* Data are numbers of patients, with percentages in parentheses.

Results

Task-based Image Quality Assessment

Table 2 shows the NPS, TTFs, and detectability indexes for the simulated lesions with the two CT systems. The noise magnitude was lower for PCCT images. The average spatial frequency of the NPS shifted toward higher frequencies for PCCT images. Two NPS peaks were found for PCCT images with spatial frequency at 0.05 mm^{-1} and 0.68 mm^{-1} (Fig E2 [online]). For both inserts, the value of TTF at 50% and 10% shifted toward higher frequencies for PCCT images. For both CT systems, higher values of TTF at 50% and 10% were found for the bone insert than for the polyethylene insert (Fig E3 [online]). The detectability indexes for PCCT images were 2.3- and 2.9-fold higher for coronary lumen and noncalcified plaque, respectively.

Clinical Study

Fourteen consecutive participants were included (mean age, 61 years ± 17; 12 men [86%]) (Fig 1, Table 3). Eight coronary segments out of 98 segments were excluded because of strong motion artifacts (five [5%] for PCCT images and three (3%) for EID DLCT images). Eight of the 14 patients (57%) had rings on PCCT images without impairment on the overall image quality. Three of the 14 patients (21%) had metallic artifacts on both PCCT and EID DLCT images.

Objective image quality analysis.—No significant difference in noise was found between PCCT and EID DLCT images (mean score, 50 ± 9 vs 43 ± 9, respectively; $P = .06$). A significant difference in vascular attenuation was found in the proximal and distal coronary lumen, with mean values greater than 350 HU (mean, 373 HU ± 140 and 359 HU

± 131, respectively for PCCT images). Beam-hardening artifact was significantly lower for PCCT images than for EID DLCT images (mean score, 8 ± 8 vs 22 ± 21, respectively; $P < .01$). With regard to differences in vascular attenuation, signal-to-noise ratios and contrast-to-noise ratios were higher for EID DLCT images ($P < .05$ for all), except for the signal-to-noise ratio in the distal coronary lumen ($P = .70$) and the contrast-to-noise ratio in the left ventricular cavity and/or aorta and cardiac muscle ($P = .13$ and $P = .09$, respectively) (Table E1 [online]). A specific objective analysis on coronary calcified plaque, showing a significant reduction of blooming artifacts with PCCT images compared with EID DLCT images (36.4% vs 48.4%, respectively; $P < .001$), is reported in Appendix E1 and Table E2 (online).

Subjective image quality analysis.—Examples of CCTA images in participants are provided in Figures 2–5.

A poor agreement (all κ values ≤0) in quality score was found between PCCT and EID DLCT images with all radiologists for overall image quality, diagnostic confidence, diagnostic quality of coronary calcification and lumen, sharpness of calcification and stent, and conspicuity of calcification and

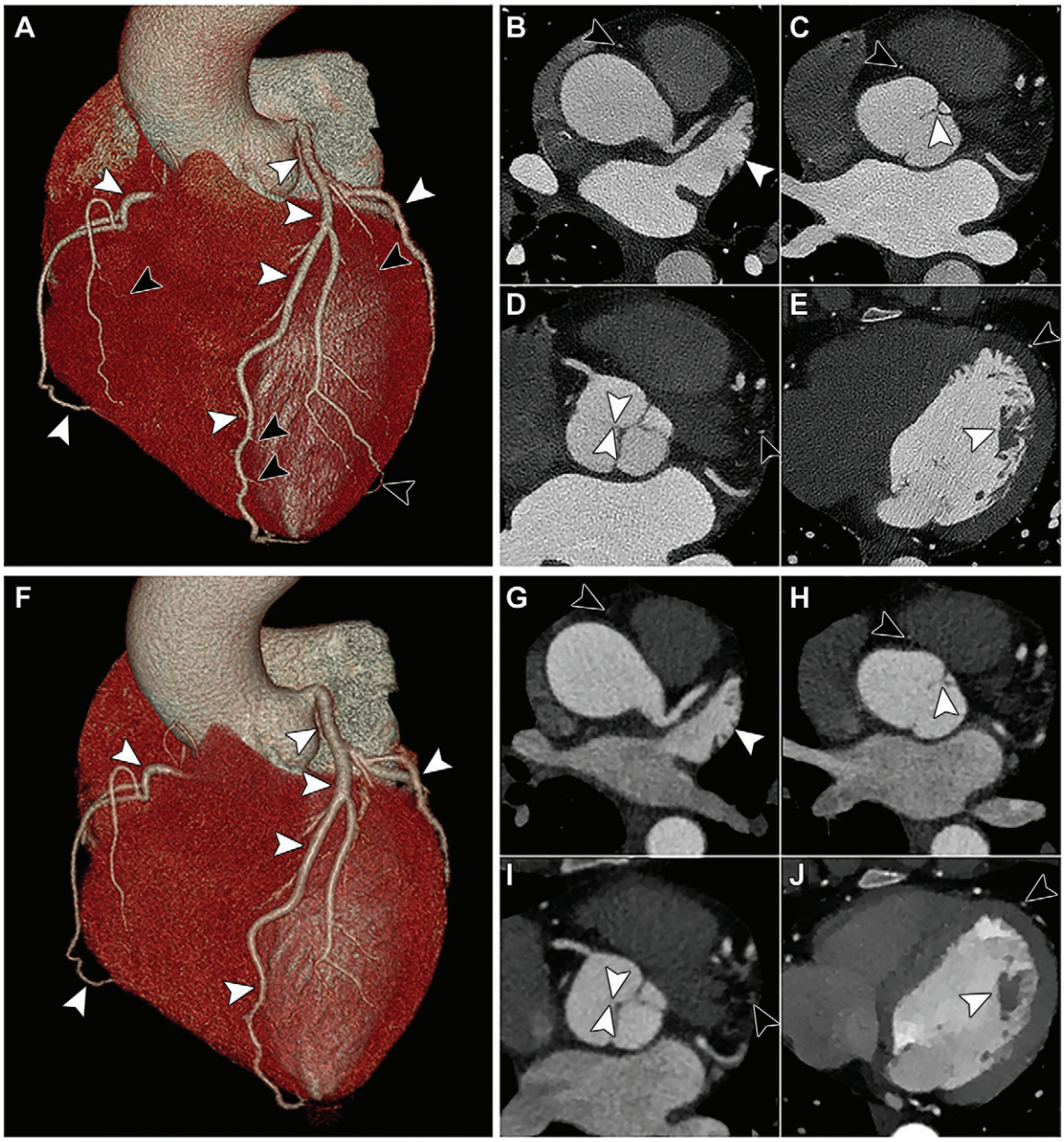

Figure 2: Images from **(A–E)** coronary photon-counting CT (PCCT) and **(F–J)** energy-integrating detector (EID) dual-layer CT (DLCT) angiography in a 44-year-old woman. Volume-rendered PCCT image (**A**) and volume-rendered EID DLCT image (**F**) depict proximal coronary arteries (white arrowheads), but there is clear improvement in the depiction of distal coronary arteries (black arrowheads in **A**) with volume rendering and PCCT in comparison to EID DLCT. On axial images, pectinate muscle (**B, G**), aortic cusp commissure (**C, H**), noncoronary cusp (**D, I**), and papillary muscle (**E, J**) were better depicted on PCCT images (**B–E**) than on EID DLCT images (**G–J**) (white arrowheads). Black arrowheads indicate distal coronary arteries not depicted on EID DLCT images.

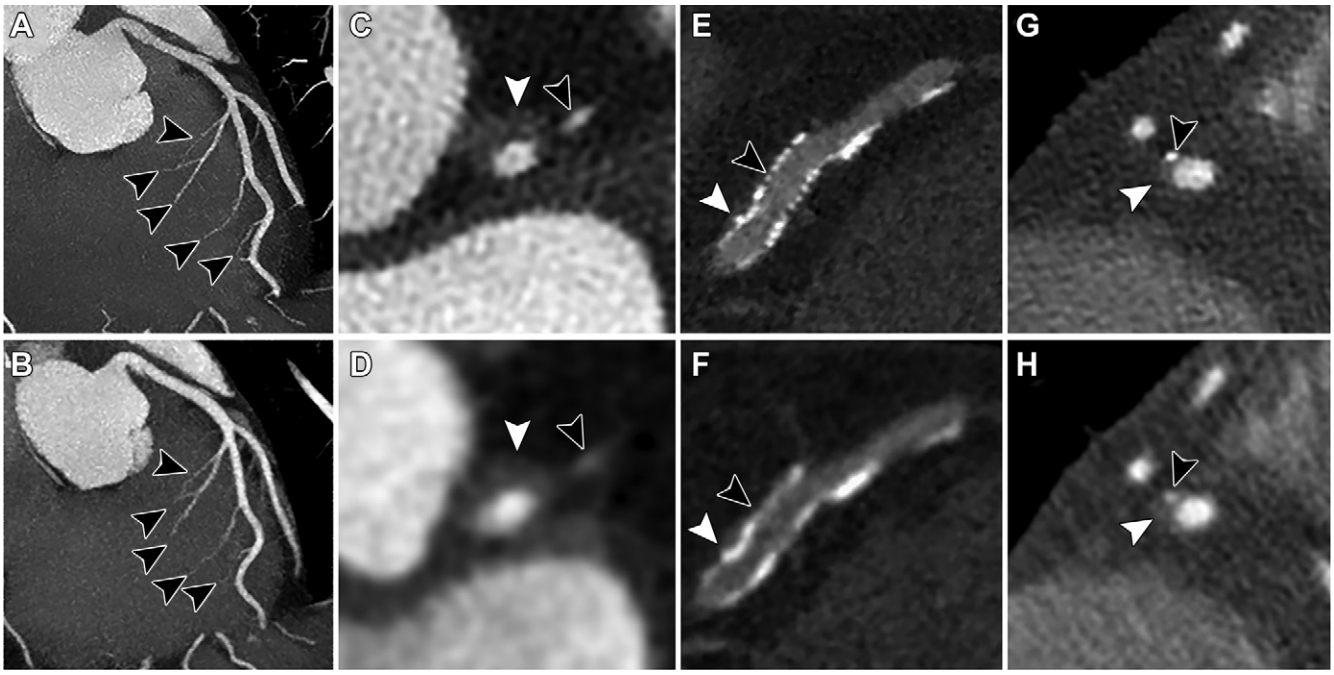

Figure 3: Images from **(A, C, E, G)** coronary photon-counting CT (PCCT) and **(B, D, F, H)** energy-integrating detector (EID) dual-layer CT (DLCT) angiography in three different patients: a 44-year-old woman (**A–D**), a 75-year-old man (**E, F**), and a 69-year-old man (**G, H**). **(A, B)** Septal branches (arrowheads) are better depicted on maximum-intensity projections with PCCT compared with EID DLCT. **(C, D)** A noncalcified plaque with positive remodeling (white arrowhead) and a small marginal branch (black arrowhead) are better depicted with PCCT than with EID DLCT. **(E, F)** A stent (black arrowhead) and an outside calcification (white arrowhead) with focal disruption of the struts are better depicted with PCCT than with EID DLCT. **(G, H)** A mixed plaque (white arrowhead) with a small calcification (black arrowhead) only differentiable from the lumen with PCCT were better depicted with PCCT than with EID DLCT.

stent. A slight agreement (κ value, 0.01–0.20) was found for the stent, noncalcified plaque, coronary wall, pericoronary fat tissue, and sharpness and conspicuity of noncalcified plaque. A moderate agreement (κ value, 0.02–0.40) was found for beam-hardening artifacts. The agreements did not differ significantly between radiologists.

The scores for overall image quality and diagnostic confidence among radiologists were higher with PCCT images, with a median score of 5 (IQR, 2) and 5 (IQR, 1), respectively, versus 4 (IQR, 1) and 4 (IQR, 3) with EID DLCT images (Table E3 [online]).

Proportions of quality score greater or equal than 4 (good) were higher for all criteria among the radiologists with PCCT images in comparison with EID DLCT images, with, for example, a proportion of 98% and 100% compared with 88% and 88% with EID DLCT images for overall quality and diagnostic confidence, respectively (Fig 6).

Proportions of score improvement with PCCT images among radiologists for overall quality and diagnostic confidence were 57% (95% CI: 41, 72) and 55% (95% CI: 39, 70), respectively, and 100%, 92% (95% CI: 71, 98), and 45% (95% CI: 28, 63) for coronary calcification, stent, and noncalcified plaque, respectively (Table 4).

Additional examples are presented in Figures E4 and E5 (online). In addition, an illustration of the multi-energy capabilities of the PCCT system through iodine and monoenergetic images at 70 and 40 keV of a coronary artery is shown in Figure E6 (online).

Radiation Dose Study

Between paired CCTA images, mean tube current (255 mAs ± 0 vs 349 mAs ± 111, respectively; $P < .01$), mean volume CT dose index (25.7 mGy vs 31.6 mGy ± 10.1, $P < .04$), and mean dose-length product (411 mGy vs 592 ± 171, $P < .01$) were significantly lower with PCCT than with EID DLCT.

Discussion

Our prospective study of participants referred for coronary CT angiography (CCTA) showed significant improvements in overall image quality, diagnostic quality, and diagnostic confidence in CCTA with photon-counting CT (PCCT) compared with an energy-integrating detector (EID) dual-layer CT (DLCT). A subjective analysis performed by three experienced cardiac radiologists showed greater overall quality and diagnostic confidence with PCCT images than with EID DLCT images, with median scores of 5 (interquartile range [IQR], 2) and 5 (IQR, 1), respectively, with PCCT images versus 4 (IQR, 1) and 4 (IQR, 3) with EID DLCT images. All three radiologists found that PCCT outperformed EID DLCT with regard to the diagnostic quality of coronary calcification, stent, and noncalcified plaque, with proportions of improvement of 100%, 92% (95% CI: 71, 98), and 45% (95% CI: 28, 63), respectively. A phantom study supported our findings as it showed up to 2.3- and 2.9-fold increased detectability index for coronary lumen and noncalcified plaque, respectively. Altogether, these key findings suggest that PCCT is a good candidate for coronary artery imaging.

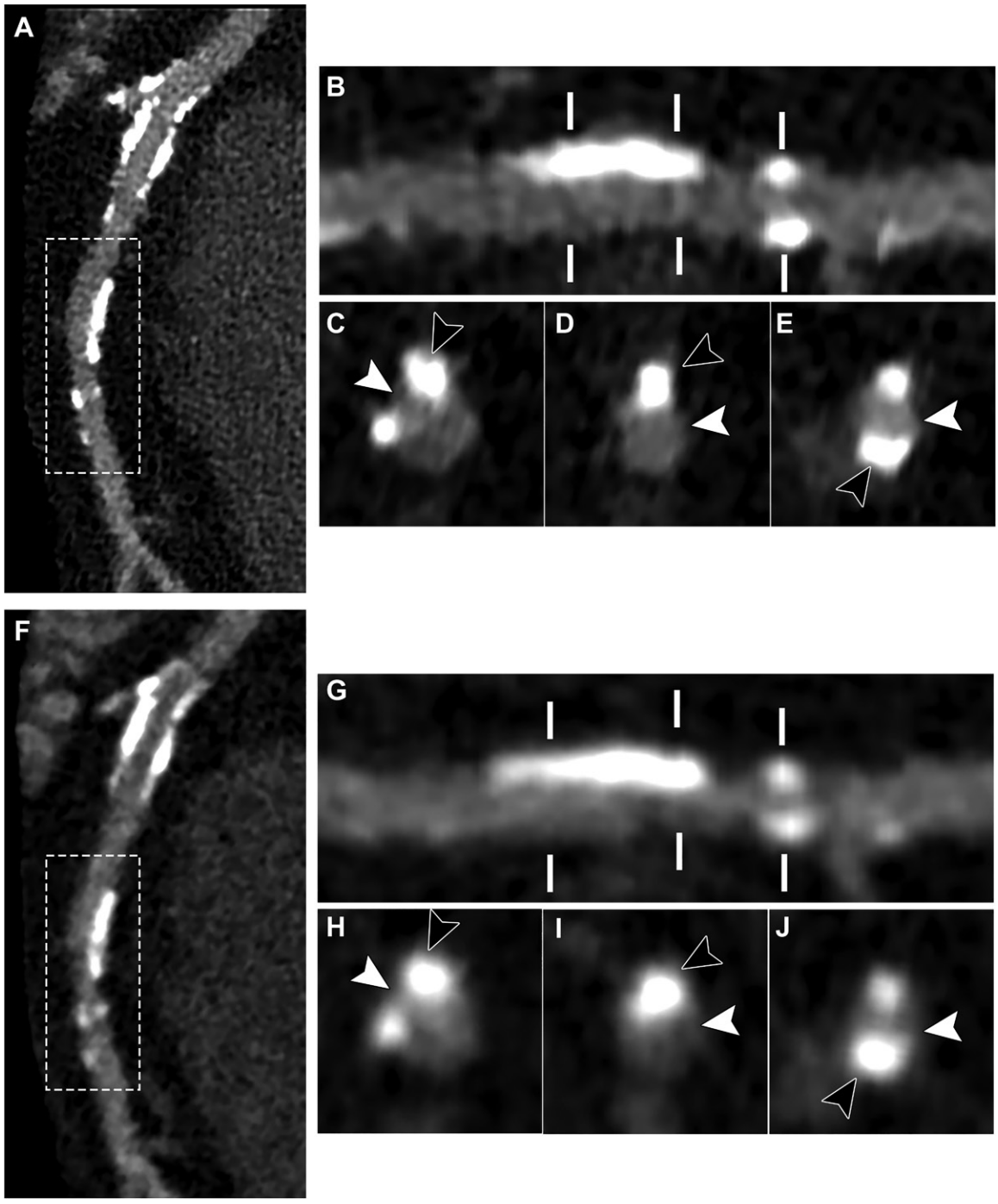

Figure 4: Images of coronary calcified plaque with **(A–E)** coronary photon-counting CT (PCCT) and **(F–J)** energy-integrating detector (EID) dual-layer CT (DLCT) angiography in a 69-year-old man. **(A, B, F, G)** Curved planar reconstructions demonstrate that calcifications (in box) are more differentiable from the lumen on PCCT images (**A, B**) than on EID DLCT images (**F, G**). **(C–E, H–J)** On cross-sectional images, the sharpness of calcifications and their impact on the lumen (white arrowhead) are better depicted with PCCT (**C–E**) than with EID DLCT (**H–J**). In addition, the lumen (black arrowhead) was also better depicted with PCCT than with EID DLCT due to the reduced blooming artifacts arising from the calcifications. In **E** (cross-sectional PCCT image), the lumen is clearly seen while in **J** (matched EID DLCT cross-sectional image), the lumen is hardly seen; this may lead to a false-negative finding of occlusion.

First, we demonstrated that PCCT images allow higher diagnostic quality, conspicuity, and sharpness of high-contrast tasks such as coronary lumen, calcification, and stent. These findings are consistent with those of recent studies that demonstrated a greater depiction of in vitro stents and coronary calcifications using a PCCT system (12,13,24–27). They are mainly explained by the gain in spatial resolution, as demonstrated by the 1.9-fold increase in the TTF values in a high-contrast insert and the shift toward higher noise frequencies for PCCT images in the phantom study. The ultra-high-resolution

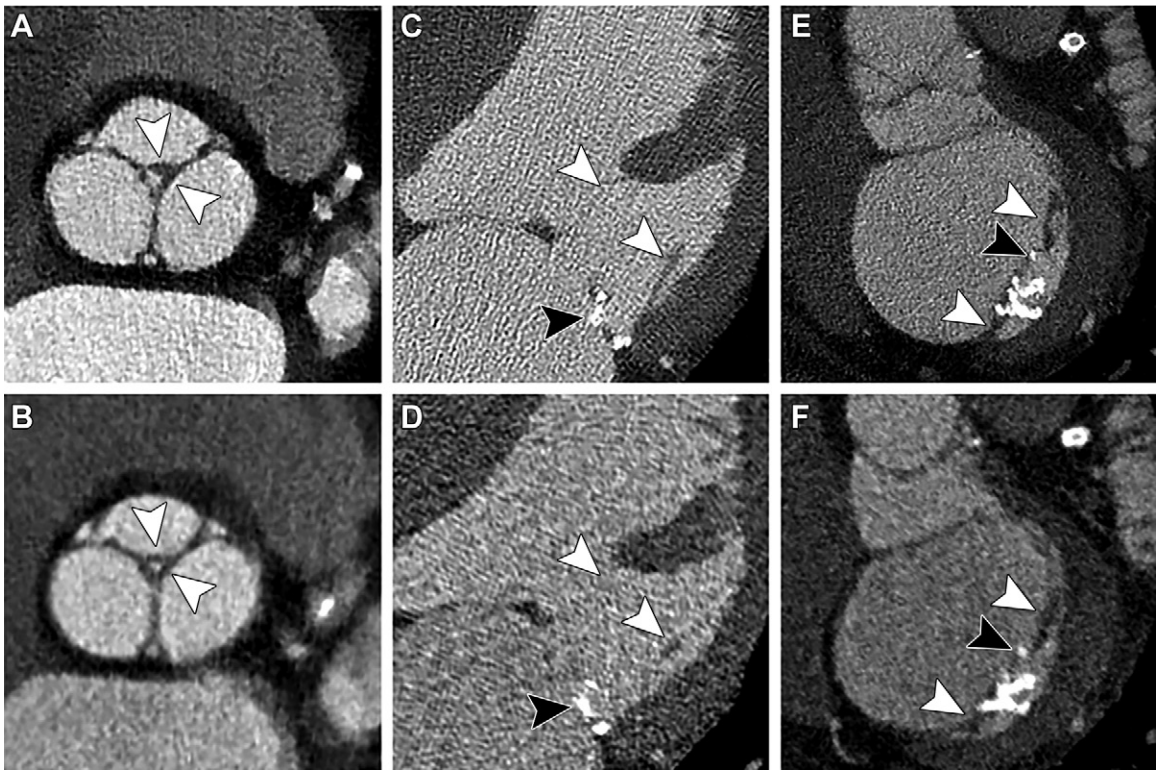

Figure 5: Images of cardiac valves with **(A, C, E)** coronary photon-counting CT (PCCT) and **(B, D, F)** energy-integrating detector (EID) dual-layer CT (DLCT) angiography in two different patients: a 52-year-old man (**A, B**) and an 86-year-old man (**C–F**). **(A, B)** Noncalcified tricuspid aortic valve is shown with better depiction of the cusps (arrowheads) with PCCT compared with EID DLCT. **(C, D)** Degenerated mitral valve is shown with better depiction of cords (white arrowheads) and calcified mural cusp (black arrowhead) with PCCT than with EID DLCT. **(E, F)** Degenerated mitral valve is shown with better depiction of a thickened mural cusp (white arrowheads) and cusp calcification burden (black arrowhead) with PCCT than with EID DLCT.

protocol of the PCCT system contributed to such results, as recently showed with conventional CT using small EIDs (28). However, this latter system cannot offer the several advantages brought by PCDs such as the energy-resolved properties and dose efficiency, which may explain a higher radiation dose burden (mean dose-length product of 678.5 mGy vs 411 mGy in the present study) (28). Interestingly, despite these ultra-high-resolution parameters that increase by definition the noise, the noise magnitude was slightly lower for PCCT images, while the magnitude of the NPS peaks was significantly lower for PCCT. This important aspect is explained by the contribution of a higher level of iterative reconstruction and also by the dose efficiency of PCDs, as previously reported in comparative studies between EID CT and PCCT systems (11,13,14). In addition, the NPS showed a shift toward high frequency for PCCT images, as previously demonstrated for ultra-high-resolution lung imaging (18), which may due to the intrinsic characteristics of PCDs and the kernel filter (10). Altogether, these are important technical aspects that help explain the high spatial resolution capabilities of the PCCT system and, consequently, the increase in detectability of high-contrast tasks.

Second, low-contrast tasks such as the visualization of noncalcified plaque were also better depicted using PCCT. This finding is supported by the phantom study that reported a 2.2-fold increase in TTF in a low-contrast insert and a lower noise magnitude with PCCT. Altogether, these resulted in an increased detectability, as previously reported for low-contrast abdominal lesions, ground-glass nodules, and low-density calcifications (18,24,29). The objective and subjective detectability improvement is explained by a better soft-tissue contrast with PCCT images, as suggested by recent studies (13,18,29). Contrary to EIDs, PCDs transmit more contrast from the low-energy photons because of the energy weighting of each incoming photon. As the linear attenuation coefficient decreases with energy, the lower energy provides more contrast. Reduction of electronic noise also contributes to this phenomenon because of the multibin capabilities of PCDs, as suggested in previous studies (11,14,18,24). This is explained by the fact that the lowest threshold is set just above the electronic noise level while with EID CT, electronic noise is added to the integrated charge (8).

Third, a reduction in metallic and beam-hardening artifacts was also observed, as previously reported with human PCCT lung imaging (11,14). The actual source of this improvement is not clear at this point, but reduction of the electronic noise and improved spatial resolution may have strongly contributed to reduce it.

In addition to the improved quality of the CAD hallmarks, the cardiac radiologists also noticed a dramatic improvement in quality for different cardiac structures such as the valves. These structures are of great interest for pre- and postprocedural CT angiography of transcatheter valve implantation and could enable a more accurate assessment in the presence

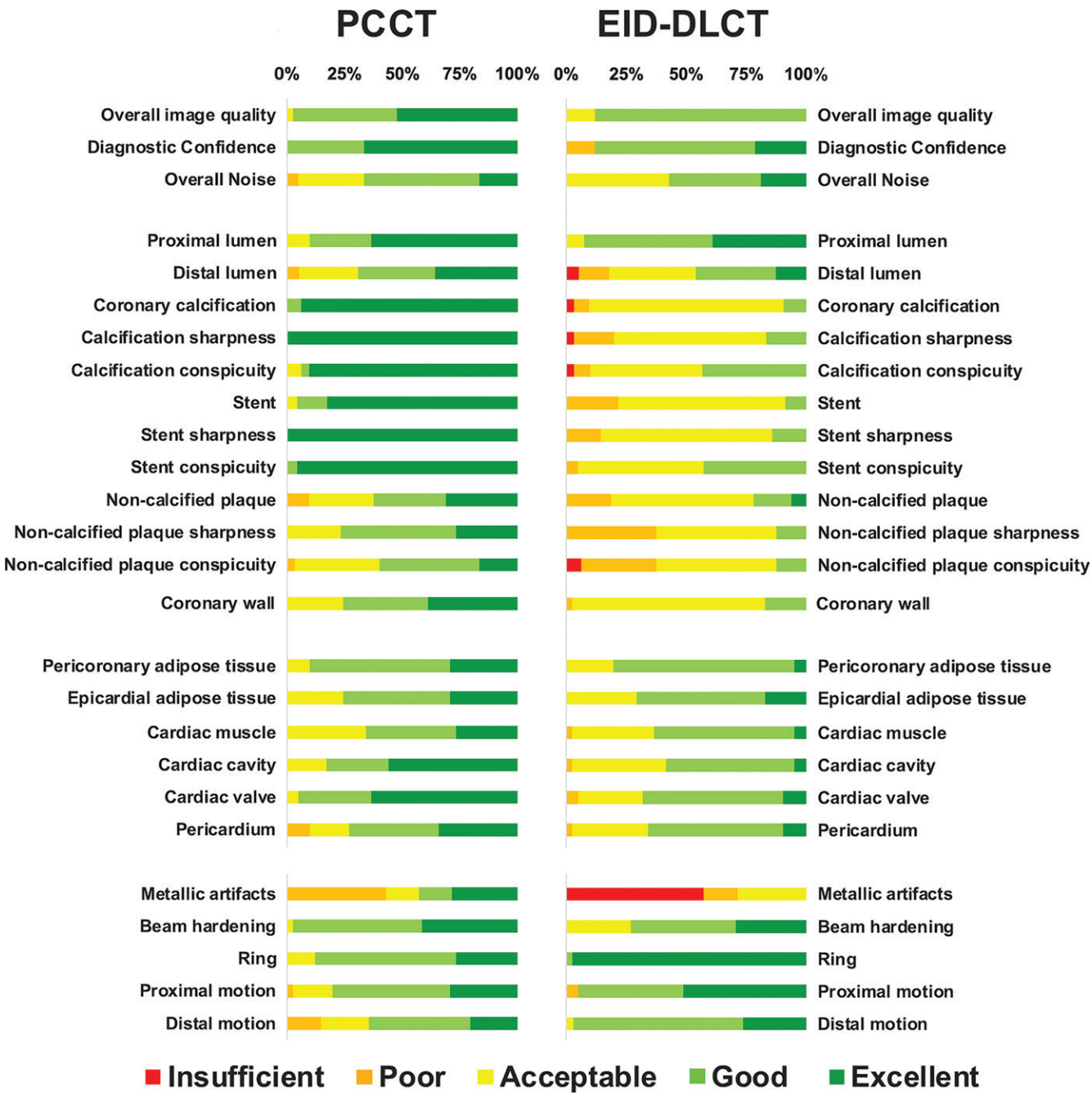

Figure 6: Plot shows results of subjective image quality analysis of images obtained with coronary photon-counting CT (PCCT) and energy-integrating detector dual-layer CT (EID-DLCT) angiography for three independent radiologists in participants with suspected or known coronary artery disease. Each bar indicates the proportion of score attributed by the radiologists for an item. Colors indicate the image quality for diagnosis: dark green indicates excellent quality; green, good quality; yellow, acceptable quality; orange, poor quality; and red, insufficient quality.

of, for example, confounding calcifications. In addition, all radiologists noticed a greater diagnostic confidence for PCCT images, with improvement for more than half of the cases, without influence from their different experience levels. This further highlights the importance of image quality improvement and brings one more stone to the promising role that PCCT may play as a tool for CAD imaging, as suggested by recent evidence for potential molecular atherosclerotic plaque characterization and K-edge imaging of coronary lumen and stents (26,30–32).

Our study has limitations. First, the number of patients was limited. Second, neither the spectral capabilities of the PCCT system nor the diagnostic accuracy for stenosis measurement were investigated. Finally, the clinical prototype PCCT system has some technical limitations: z-coverage of 1.76 cm, rotation time of 0.33 second, pitch of 0.32, and absence of bolus test protocol and dose modulation. These factors, in particular the different bolus timing techniques, may have contributed to the difference in scanning timing relative to the contrast material injection. Consequently, they may explain the difference in

Table 4: Proportions of Improvement in Quality Score and Their 95% CIs with Coronary PCCT versus EID DLCT

Criterion	Proportions of Improvement (%)	95% CI
Overall image quality	57	41, 72
Diagnostic confidence	55	39, 70
Overall noise	26	15, 42
Diagnostic quality		
Coronary calcifications	100	NA
Stent	92	71, 98
Coronary noncalcified plaque	45	28, 63
Coronary proximal lumen	48	33, 63
Coronary distal lumen	51	35, 67
Coronary wall	69	53, 82
Pericoronary fat tissue	36	22, 52
Sharpness		
Coronary calcifications	100	NA
Stent	100	NA
Coronary noncalcified plaque	68	48, 83
Conspicuity		
Coronary calcifications	94	77, 99
Stent	100	NA
Coronary noncalcified plaque	57	38, 74
Beam-hardening artifacts	33	20, 49

Note.—Data were calculated from three radiologists. DLCT = dual-layer CT, EID = energy-integrating detector, NA = not applicable, PCCT = photon-counting CT.

vascular attenuation and as a result signal-to-noise and contrast-to-noise ratios. However, these limitations are expected to be addressed in the near future, projecting further improvements to image quality and radiation dose.

In conclusion, the photon-counting CT system outperformed an energy-integrating detector dual-layer CT system in improving image quality and diagnostic confidence of coronary CT angiography, representing a step forward in realizing the promise of this technology for coronary artery disease imaging.

Acknowledgments: We are deeply grateful to Hélène De Forges, PhD, for her help in editing the manuscript, and Cyril Prieur, MD, and Ahmad Hayek, MD, for their help in patient enrollment.

Author contributions: Guarantors of integrity of entire study, **S.A.S.M., A.D., M.V., P.C.D.**; study concepts/study design or data acquisition or data analysis/interpretation, all authors; manuscript drafting or manuscript revision for important intellectual content, all authors; approval of final version of submitted manuscript, all authors; agrees to ensure any questions related to the work are appropriately resolved, all authors; literature research, **S.A.S.M., S.B., A.D., M.V., P.A.R., R.D., J.G., P.C.D.**; clinical studies, **S.A.S.M., S.B., H.L., A.D., M.V., P.A.R., R.D., M.V., T.B., G.F., C.B., P.C.D.**; experimental studies, **S.A.S.M., S.B., A.D., M.V., P.A.R., R.D., E.L., K.E., E.B., G.F., J.G.**; statistical analysis, **S.A.S.M., S.B., H.L., A.D., M.V., B.R.**; and manuscript editing, **S.A.S.M., S.B., H.L., A.D., M.V., P.A.R., R.D., M.V., V.T.L., T.B., P.C., Y.Y., B.R., E.B., G.R., C.B., L.B., J.G., P.C.D.**

Disclosures of conflicts of interest: S.A.S.M. Payment for presentations by Boehringer. **S.B.** No relevant relationships. **H.L.** No relevant relationships. **A.D.** No relevant relationships. **M. Varasteh** No relevant relationships. **P.A.R.** No relevant relationships. **R.D.** No relevant relationships. **M. Villien** No relevant relationships. **V.T.L.** No relevant relationships. **T.B.** No relevant relationships. **P.C.** No relevant relationships. **Y.Y.** No relevant relationships. **E.L.** No relevant relationships. **K.E.** No relevant relationships. **B.R.** No relevant relationships. **E.B.** No relevant relationships. **G.R.** No relevant relationships. **G.F.** No relevant relationships. **C.B.** Consulting fees from Bayer, Amgen, Sanofi, and Servier. **L.B.** No relevant relationships. **J.G.** No relevant relationships. **P.C.D.** No relevant relationships.

References

1. Dweck MR, Maurovich-Horvat P, Leiner T, et al. Contemporary rationale for non-invasive imaging of adverse coronary plaque features to identify the vulnerable patient: a Position Paper from the European Society of Cardiology Working Group on Atherosclerosis and Vascular Biology and the European Association of Cardiovascular Imaging. Eur Heart J Cardiovasc Imaging 2020;21(11):1177–1183.
2. Abbara S, Blanke P, Maroules CD, et al. SCCT guidelines for the performance and acquisition of coronary computed tomographic angiography: A report of the society of Cardiovascular Computed Tomography Guidelines Committee: Endorsed by the North American Society for Cardiovascular Imaging (NASCI). J Cardiovasc Comput Tomogr 2016;10(6):435–449.
3. Greenland P, Alpert JS, Beller GA, et al. 2010 ACCF/AHA guideline for assessment of cardiovascular risk in asymptomatic adults: a report of the American College of Cardiology Foundation/American Heart Association Task Force on Practice Guidelines. J Am Coll Cardiol 2010;56(25):e50–e103.
4. Raff GL, Chinnaiyan KM, Cury RC, et al. SCCT guidelines on the use of coronary computed tomographic angiography for patients presenting with acute chest pain to the emergency department: a report of the Society of Cardiovascular Computed Tomography Guidelines Committee. J Cardiovasc Comput Tomogr 2014;8(4):254–271.
5. Knuuti J, Wijns W, Saraste A, et al. 2019 ESC Guidelines for the diagnosis and management of chronic coronary syndromes. Eur Heart J 2020;41(3):407–477.
6. SCOT-HEART Investigators; Newby DE, Adamson PD, et al. Coronary CT Angiography and 5-Year Risk of Myocardial Infarction. N Engl J Med 2018;379(10):924–933.
7. Hoffmann U, Truong QA, Schoenfeld DA, et al. Coronary CT angiography versus standard evaluation in acute chest pain. N Engl J Med 2012;367(4):299–308.
8. Taguchi K, Iwanczyk JS. Vision 20/20: Single photon counting x-ray detectors in medical imaging. Med Phys 2013;40(10):100901.
9. Si-Mohamed S, Bar-Ness D, Sigovan M, et al. Review of an initial experience with an experimental spectral photon-counting computed tomography system. Nucl Instrum Methods Phys Res Sect Accel Spectrometers Detect Assoc Equip 2017;873:27–35.
10. Blevis I. X-Ray Detectors for Spectral Photon Counting CT. In: Taguchi K, Blevis I, Iniewski K, eds. Spectral, Photon Counting Computed Tomography: Technology and Applications. Boca Raton, Fla: CRC Press, 2020; 179–190.
11. Si-Mohamed S, Boccalini S, Rodesch PA, et al. Feasibility of lung imaging with a large field-of-view spectral photon-counting CT system. Diagn Interv Imaging 2021;102(5):305–312.
12. Boccalini S, Si-Mohamed S, Dessouky R, Sigovan M, Boussel L, Douek P. Feasibility of human vascular imaging of the neck with a large field-of-view spectral photon-counting CT system. Diagn Interv Imaging 2021;102(5):329–332.
13. Symons R, Sandfort V, Mallek M, Ulzheimer S, Pourmorteza A. Coronary artery calcium scoring with photon-counting CT: first in vivo human experience. Int J Cardiovasc Imaging 2019;35(4):733–739.
14. Symons R, Pourmorteza A, Sandfort V, et al. Feasibility of dose-reduced chest CT with photon-counting detectors: initial results in humans. Radiology 2017;285(3):980–989.
15. Si-Mohamed S, Boussel L, Douek P. Clinical Applications of Spectral Photon-Counting CT. In: Taguchi K, Blevis I, Iniewski K, eds. Spectral, Photon Counting Computed Tomography: Technology and Applications. Boca Raton, Fla: CRC Press, 2020; 97–116.
16. Steadman R, Herrmann C, Livne A. ChromAIX2: A large area, high count-rate energy-resolving photon counting ASIC for a spectral CT prototype. Nucl Instrum Methods Phys Res 2017;862:18–24.
17. Samei E, Richard S. Assessment of the dose reduction potential of a model-based iterative reconstruction algorithm using a task-based performance metrology. Med Phys 2015;42(1):314–323.
18. Si-Mohamed SA, Greffier J, Miailhes J, et al. Comparison of image quality between spectral photon-counting CT and dual-layer CT for the evaluation of lung nodules: a phantom study. Eur Radiol 2021. 10.1007/s00330-021-08103-5. Published online June 29, 2021.

19. Greffier J, Hamard A, Pereira F, et al. Image quality and dose reduction opportunity of deep learning image reconstruction algorithm for CT: a phantom study. Eur Radiol 2020;30(7):3951–3959.
20. Greffier J, Frandon J, Larbi A, Om D, Beregi JP, Pereira F. Noise assessment across two generations of iterative reconstruction algorithms of three manufacturers using bone reconstruction kernel. Diagn Interv Imaging 2019;100(12):763–770.
21. Greffier J, Frandon J, Larbi A, Beregi JP, Pereira F. CT iterative reconstruction algorithms: a task-based image quality assessment. Eur Radiol 2020;30(1):487–500.
22. Greffier J, Boccalini S, Beregi JP, et al. CT dose optimization for the detection of pulmonary arteriovenous malformation (PAVM): A phantom study. Diagn Interv Imaging 2020;101(5):289–297.
23. Greffier J, Frandon J, Si-Mohamed S, et al. Comparison of two deep learning image reconstruction algorithms in chest CT images: A task-based image quality assessment on phantom data. Diagn Interv Imaging 2021. 10.1016/j.diii.2021.08.001. Published online September 5, 2021.
24. van der Werf NR, Si-Mohamed S, Rodesch PA, et al. Coronary calcium scoring potential of large field-of-view spectral photon-counting CT: a phantom study. Eur Radiol 2021. 10.1007/s00330-021-08152-w. Published online July 13, 2021.
25. Bratke G, Hickethier T, Bar-Ness D, et al. Spectral Photon-Counting Computed Tomography for Coronary Stent Imaging: Evaluation of the Potential Clinical Impact for the Delineation of In-Stent Restenosis. Invest Radiol 2020;55(2):61–67.
26. Sigovan M, Si-Mohamed S, Bar-Ness D, et al. Feasibility of improving vascular imaging in the presence of metallic stents using spectral photon counting CT and K-edge imaging. Sci Rep 2019;9(1):19850.
27. Mannil M, Hickethier T, von Spiczak J, et al. Photon-Counting CT: High-Resolution Imaging of Coronary Stents. Invest Radiol 2018;53(3):143–149.
28. Latina J, Shabani M, Kapoor K, et al. Ultra-High-Resolution Coronary CT Angiography for Assessment of Patients with Severe Coronary Artery Calcification: Initial Experience. Radiol Cardiothorac Imaging 2021;3(4):e210053.
29. Gutjahr R, Halaweish AF, Yu Z, et al. Human imaging with photon counting-based computed tomography at clinical dose levels: contrast-to-noise ratio and cadaver studies. Invest Radiol 2016;51(7):421–429.
30. Si-Mohamed SA, Sigovan M, Hsu JC, et al. In Vivo Molecular K-Edge Imaging of Atherosclerotic Plaque Using Photon-counting CT. Radiology 2021;300(1):98–107.
31. Feuerlein S, Roessl E, Proksa R, et al. Multienergy photon-counting K-edge imaging: potential for improved luminal depiction in vascular imaging. Radiology 2008;249(3):1010–1016.
32. Leiner T. A New Era in Atherosclerotic Plaque Characterization with Photon-counting CT. Radiology 2021;300(1):108–109.
33. Boccalini S, den Harder AM, Witsenburg M, et al. Computed tomography image quality of aortic stents in patients with aortic coarctation: a multicentre evaluation. Eur Radiol Exp 2018;2(1):17.